Layer interface effects on dielectric breakdown strength of 3D printed rubber insulator using stereolithography

Muneaki Kurimoto[a,*], Yuya Manabe[b], Shinichi Mitsumoto[c], Yasuo Suzuoki[d]

[a] Nagoya University, Nagoya, Aichi, 464-8603, Japan

[b] Chubu Electric Power Co., Inc. , Nagoya, Aichi, 459-8522, Japan

[c] National Institute of Technology, Toyota College, Toyota, Aichi, 471-8525, Japan

[d] Aichi Institute of Technology, Toyota, Aichi, 470-0392, Japan

*Corresponding author. Email address: kurimoto@nuee.nagoya-u.ac.jp

Keywords: dielectric breakdown strength, rubber insulator, layer interface, stereolithography

Abstract

The use of 3D printing technology enables the fabrication of optimally shaped and functionally graded structured high-voltage solid insulators that could be used efficiently in power grids owing to their compact size and reliability. However, understanding the layer interface effect is challenging. Therefore, we investigated the layer interface effect on the dielectric breakdown strength of 3D printed rubber insulators. We fabricated acrylic rubber insulators in different laminate directions using a stereolithographic 3D printer. The breakdown test revealed that a layer interface with a 0.1 mm laminating pitch reduced the AC breakdown strength of the insulators. Further, we evaluated the morphology of the layer interface and the surrounding hardness using microscopic and nanoindentation analyses. We found no delamination or voids around the layer interface. However, differences in hardness between the layer interface and the other part were observed. Therefore, it was concluded that owing to insufficient curing around the layer interfaces, the difference in the material structure promoted dielectric breakdown. Consequently, to minimize the layer interface effect on the breakdown strength, we proposed a thinner layer and 3D cylindrical printings.

1. Introduction

Additive manufacturing (AM) is a process of joining materials, usually layer-upon-layer, to create an object from three-dimensional (3D) model data [1–6]. The materials used for AM include metal, polymer, and polymer composites filled with ceramic particles [7–12]. Thus, the mechanical, electrical, and thermal strengths of the materials are similar to practical levels. A 3D printer, used for the AM process, can develop complex structures with optimized physical properties, such as topology optimization and functionally graded material [13–19].

Recently, the study of 3D printed high-voltage insulators, such as bushing of power transmission systems, an insulating spacer in power circuit breakers, and a rubber insulator in cable termination, have been conducted. An insulating spacer model comprising acrylic resin filled with Al_2O_3 particles was fabricated using a stereolithographic 3D printer [20]. Further, a conductivity-graded spacer model was produced using a fused deposition modeling printer [21]. The high-voltage performance of the printed models was verified. However, the technical hindrance to realizing such progress is a proper understanding of the layer interface effects, which are structures peculiar to that of a 3D-printed solid insulator. Previous studies have reported that the layer interface reduces the breakdown strength of the insulator [22–24]. These 3D-printed insulators comprise hard solids [20–24]. Nevertheless, few studies have been conducted on 3D-printed solid insulators developed from soft solids (such as rubber).

In this study, we investigated the layer interface effect on the dielectric breakdown strength of an insulator made of rubber. The sheet samples made of acrylic rubber with different laminate directions were fabricated using a stereolithographic 3D printer, and their AC breakdown strength was evaluated using a McKeown electrode. The morphology of the layer interfaces and the hardness surrounding interface were evaluated using microscopic and nanoindentation analyses. Based on these results, a mechanism for the layer interface effects

on the breakdown strength was discussed, and 3D printing methods that minimize the layer interface effect were demonstrated.

2. Material and methods

2.1 Stereolithographic 3D printer

Stereolithography [25–27] is a highly accurate 3D printing technique, which prints 3D objects by stacking thin layers of UV-curable polymers (such as acrylic resin and rubber) and curing them under UV light radiation. However, certain properties of UV-curable polymers (such as weather and crack resistance) could be improved. Stereolithographic 3D printers can produce solid insulators without voids, which are critical defects that need to be avoided in high-voltage insulators.

Fig. 1 shows a schematic of the stereolithographic 3D printer (Form2, Formlabs) used in this study. The UV-curable polymer filled in a transparent tray was partially cured using a UV laser ($\lambda = 405$ nm) through the tray bottom. While the building plate was elevated step-by-step, the polymer was cured layer-by-layer. We used a laminating pitch formed in steps of 0.05 and 0.1 mm.

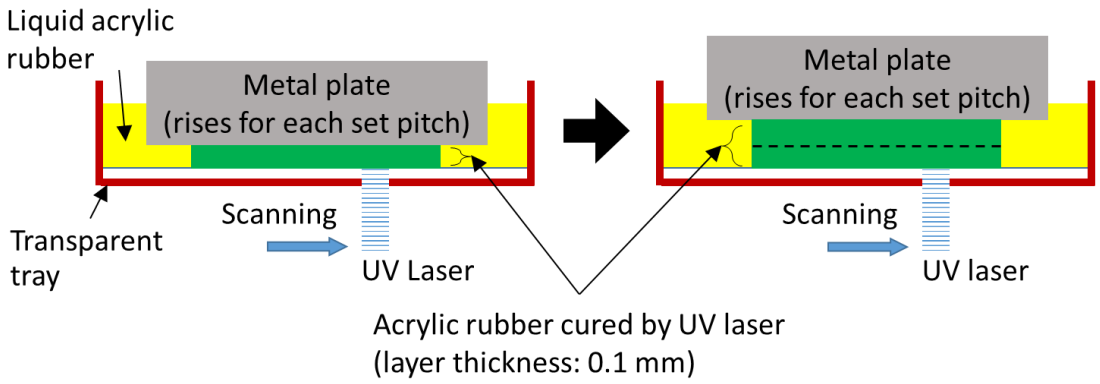

Fig. 1 A schematic of the stereolithographic 3D printer.

2.2 Material and sample preparation

The material used in the stereolithographic 3D printer was acrylic rubber (Flexible, Formlab, inc), with the following mechanical properties: tensile strength = 3.3–3.4 MPa and softening point = 231 °C. The insulator was thermally cured. Fig. 2 depicts a column insulator (diameter: 30 mm, height: 30 mm) prepared using the stereolithographic 3D printer. Two-column insulators, one laminated in the direction of the column height (Print H), while the other laminated in the vertical direction of Print H (Print V), were prepared. Print H_0.1mm and Print V_0.1mm denote the column insulators, each with a laminating pitch of 0.1 mm. We prepared a column insulator with no laminate interface (Mold), using the same molding process, to compare it with the laminated insulator. The polymers were poured into the mold and cured by UV light. The specimen was post-cured thermally at 70 degrees celsius. To evaluate the breakdown strength, we prepared a sheet sample by slicing the column insulators (thickness = 0.3–0.6 mm), as shown in Fig. 3.

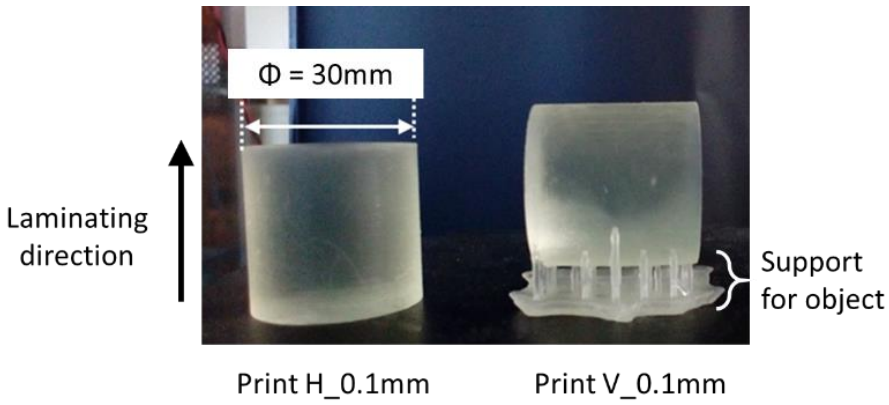

Fig. 2. Column insulators (diameter: 30 mm, height: 30 mm) were prepared using the stereolithographic 3D printer.

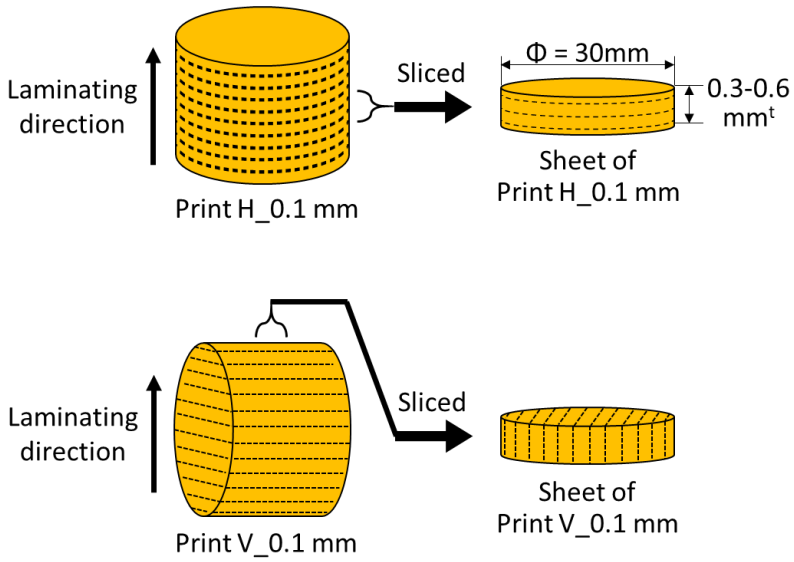

Fig.3 A sheet sample (thickness = 0.3–0.6 mm) formed by slicing the column insulators.

2.3 Dielectric breakdown test for solid part

In general, the breakdown strength of the insulating material is evaluated using mold-type electrodes, such as a recessed electrode or a McKeown electrode [28]. Fig. 4 illustrates a McKeown electrode. The mold-type electrode is different from the ASTM D149 standard electrode [29]. In the former, the sheet sample and the electrode are covered with a solid resin to avoid discharge on the sample surface, enabling the measurement of the strength of the solid part. In contrast, in the latter, the sheet sample and electrode are covered with insulating oil, allowing creepage discharge to occur on the surface. Thus, the measurement of the breakdown strength of both the solid part and the surface is enabled.

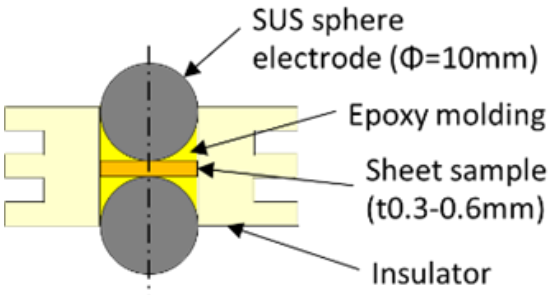

Fig. 4 A McKeown electrode

The breakdown test was carried out using a McKeown electrode. The sheet sample was sandwiched between two electrodes (diameter: 10 mm) and then sealed with an insulating resin. The number of the sheet samples was 9-10. Then, a 60 Hz AC voltage was applied, at an increasing rate of 1 kVp/s, across the McKeown electrode immersed in the insulating oil. The breakdown strength was determined by dividing the breakdown voltage by the sheet thickness.

2.4 Microscope observation and hardness evaluation

For morphological analysis of the layer interfaces, the cross-section of the sheet was observed using a polarized light microscope and a scanning electron microscope (SEM). Further, to avoid filling the defects (such as voids and cracks with polishing powders or polishing residues), the cross-section was polished using the Cryo-IP method. Here, the surface atoms were ejected by irradiating an argon-ion beam while cooling the sample. For SEM observation, the cross-section was treated with a conductive coating.

To evaluate the hardness in the vicinity of the layer interface, we used nanoindentation measurements (Triboindenter TI 950 from Hysitron) by pressing the nanoindenter against the region near the layer interface (on the sample's cross-section). The Barkovich indenter cross-section and the maximum indentation depth used in this study were 24.5 μm^2 and 1 μm, respectively.

3. Results and discussion

3.1 Effect of laminating direction on AC breakdown strength

Fig. 5 shows the AC breakdown strengths of Mold, Print H_0.1mm, and Print V_0.1mm. The breakdown strength of Print H_0.1mm was higher than that of Print V_0.1mm, both of which were lower than that of Mold. The layer interfaces reduced the breakdown strength. In particular, the layer interface parallel to the electric field direction enhanced the reduction in breakdown voltage.

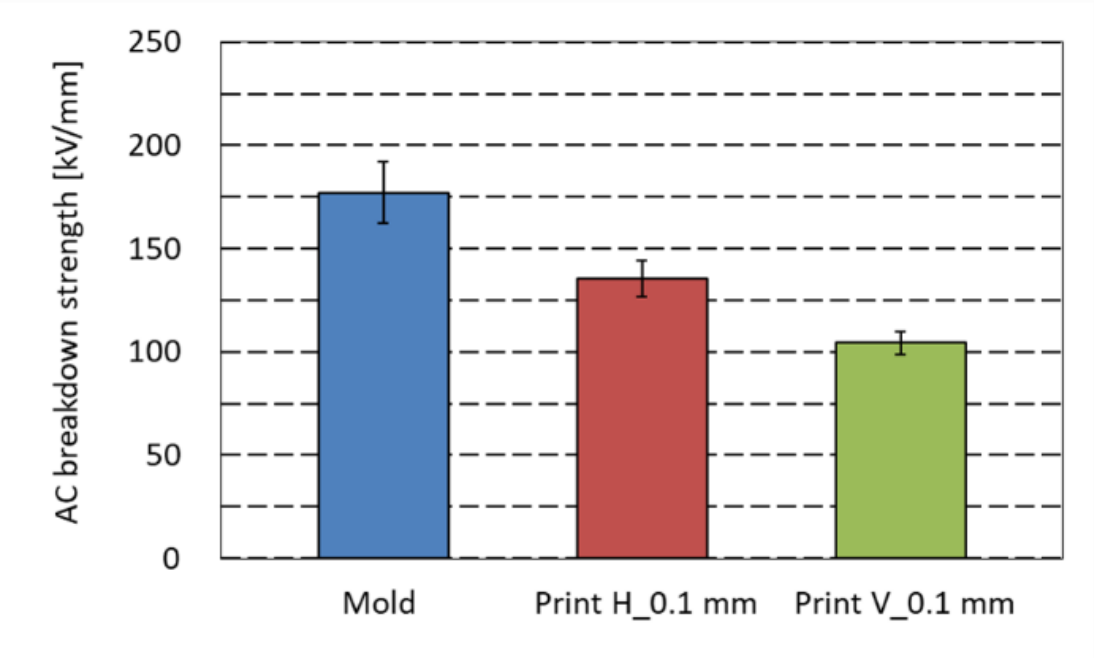

Fig. 5 AC breakdown strengths of Mold, Print H_0.1mm, and Print V_0.1mm.

To further verify the breakdown strength data, we adopted a statistical approach using the Weibull distribution [30,31] (Fig. 6). Each plot evinced a straight line, indicating that the breakdown phenomena of Mold, Print H_0.1 mm, and Print V_0.1 mm agreed with Weibull probability. The inclinations of Print H_0.1mm and Print V_0.1mm were similar to those of Mold. It was observed that the layer interface, with a laminating pitch of 0.1 mm, weakened the breakdown strength of the insulator, rather than inducing a stochastic defect, that is, delamination or voids.

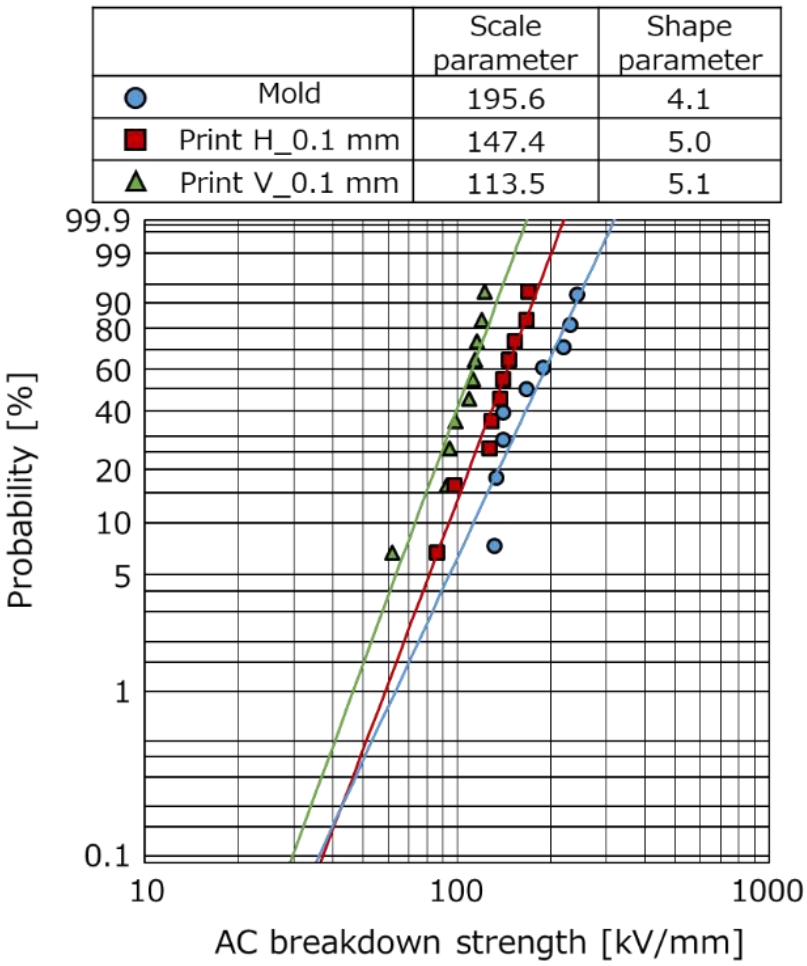

Fig. 6 Weibull distribution of AC breakdown strengths of Mold, Print H_0.1mm, and Print V_0.1mm.

3.2 Morphology of layer interfaces

Fig. 7 shows a polarizing microscope image of the Print H_0.1mm cross-section. The cross-section is in the thickness direction. The layer interfaces at a laminating pitch of 0.1 mm were observed. In general, the contrast in the images depends on the refractive index of the material, and the refractive index of acrylic rubber depends on the material structure. The different contrast in the interface images indicate differences in the material structure of the other part. Through SEM analysis, we checked the layer interfaces for any nanometric defects. Fig. 8 shows the SEM images of the cross-section around the layer interface, as shown in Fig.7. The enlarged region of Fig. 8 (a) is shown in Fig.8 (b). We observed no delamination or voids larger than the nanometric size around the layer interfaces.

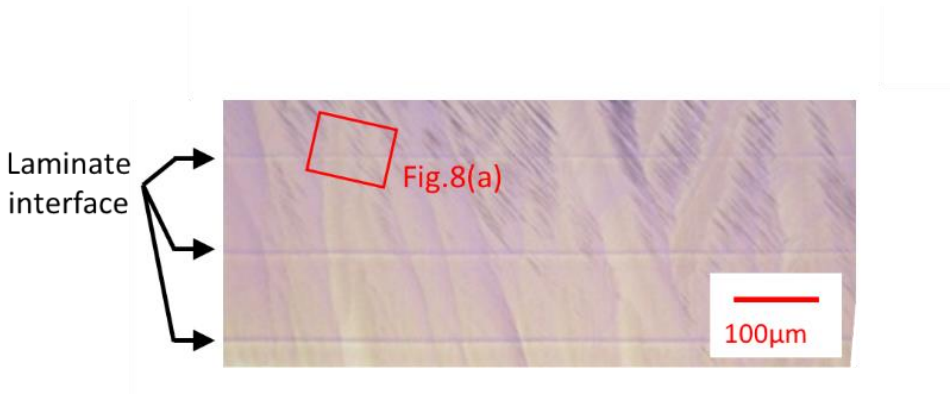

Fig. 7 A polarized light microscope cross-sectional image of Print H_0.1mm.

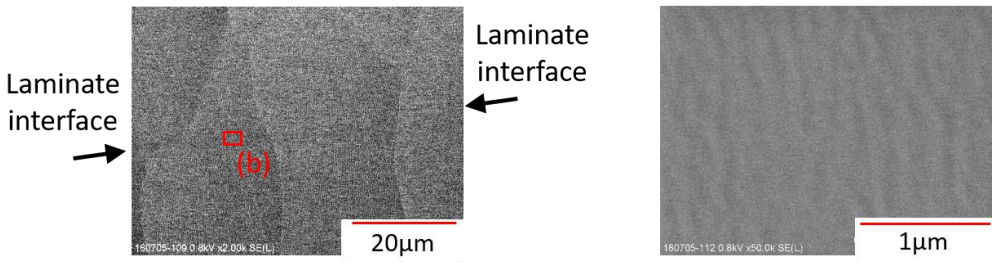

(a) Interface (b) Enlarged part of (a)

Fig. 8 SEM images of the cross-section around the layer interface shown in Fig.7.

3.3 Nanoindentation hardness around layer interfaces

The hardness in the vicinity of the layer interfaces was evaluated using nanoindentation measurements to understand the cause of the difference in the material structure around the layer interfaces. Fig. 9(a) and (b) show the observation points and hardness values, respectively. The hardness of the layer interface was higher than that of the central part between the layer interfaces. The hardness of the acrylic rubber depends on the curing degree. It indicates that the laminate interface has a peculiar material structure. Therefore, the cure degree of the central part was lower than that of the layer interfaces.

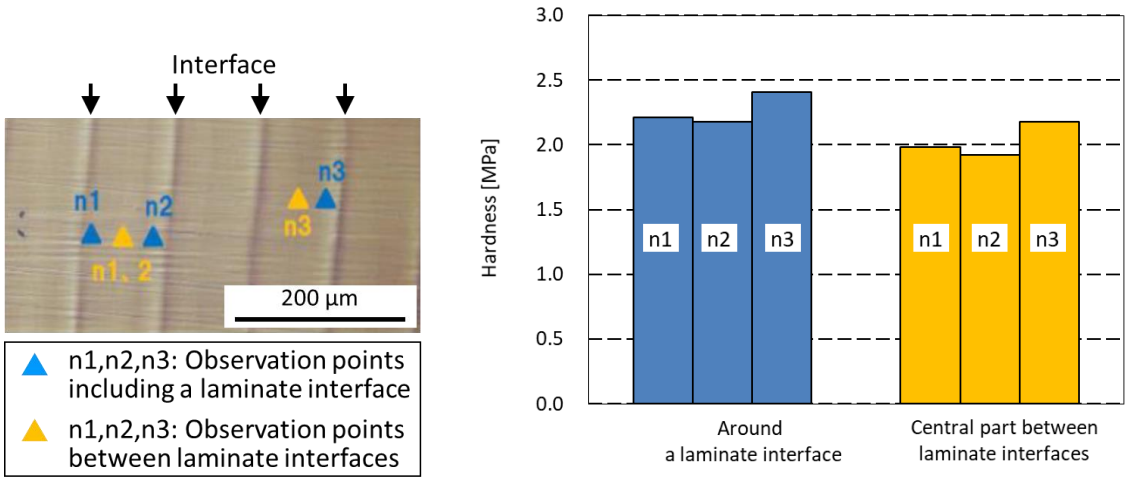

(a) Observation points (b) Hardness

Fig. 9 Observation points and the hardness values in the vicinity of the layer interfaces of Print V_0.1mm.

3.4 Emerging mechanism of layer interfaces and the effect on breakdown strength

A conceptual diagram depicting the possible mechanism of the emerging curing degree of the 3D-printed rubber insulator is shown in Fig. 10. After UV irradiation, the cure degree of the lower part of the 0.1-mm-thick layer, close to the laser, was sufficient. In contrast, the cure degree of the upper part was insufficient, which is attributed to the absorption of UV light by the sufficiently cured part, suppressing the photopolymerization of the upper part.

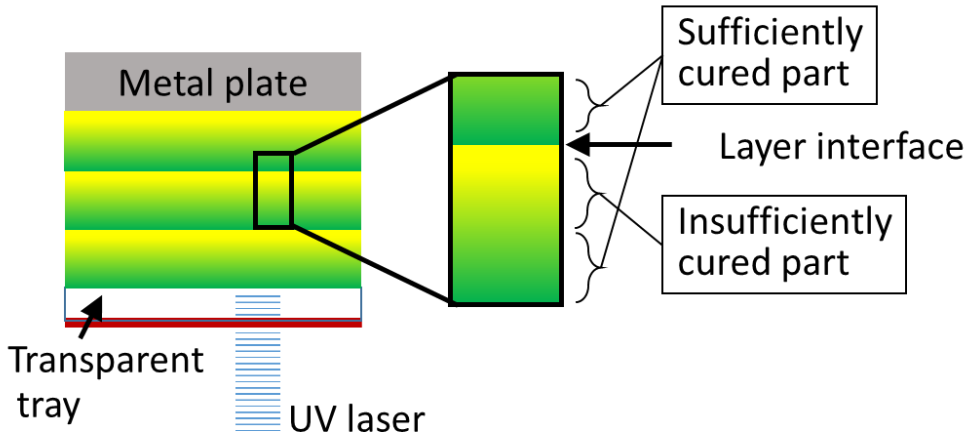

Fig.10 Conceptual diagram depicting the possible mechanism of the emerging curing degree of the 3D-printed rubber insulator.

Fig. 11 shows the conceptual diagram of the breakdown path through the layer interfaces of Print V_0.1mm. In the insufficiently cured region of the acrylic rubber, the unbonded molecules are mobile ions and/or free volume voids [32] exist. In general, movable ions increase electrical conductivity, so that the generated joule heat induces dielectric breakdown. In free volume voids, electrons easily move and electron avalanches occur, resulting in the low breakdown strength [33]. It is assumed that the insufficiently cured region has low breakdown strength and high electrical conductivity. The electric field applied across the insufficiently cured part in Print H_0.1mm is lower than the average electric field because of the Maxwell-

Wagner effect, while the electric field in the insufficiently cured part in Print V_0.1mm is the average electric field. Therefore, Print V_0.1mm shows a lower breakdown voltage than Print H_0.1mm. The direction of the layer interfaces is parallel to the electric field direction, resulting in the central part of the layer interface becoming a breakdown path. This observation is consistent with the statistical interpretation of the breakdown strength (section 3.1).

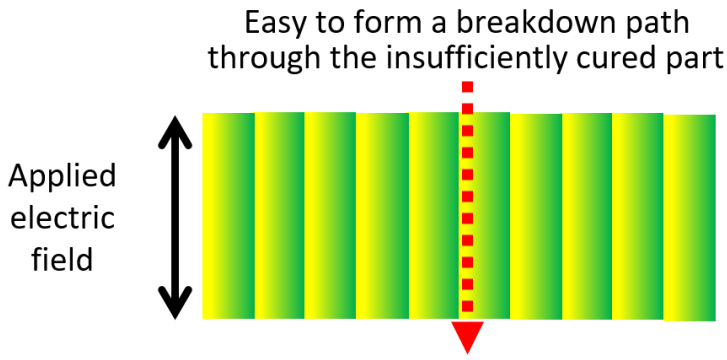

Fig. 11 The conceptual diagram of a breakdown path through the layer interfaces of Print V_0.1mm.

3.5 Minimizations of layer interface effect

3.5.1 Thinner layer printing

Lowering the laminating pitch was expected to permit irradiation of the entire acrylic rubber layer by a UV laser, ensuring sufficient curing of the acrylic rubber layer. Thin layer samples with a laminating pitch of 0.05 mm were prepared using the same method. They are denoted as Print H_0.05 mm and Print V_0.05 mm, respectively.

Fig. 12 shows that the AC breakdown strengths of Print H_0.05mm and Print V_0.05mm were higher than those of Mold, Print H_0.1mm, and Print V_0.1mm. The normalized breakdown strength was obtained from the average AC breakdown strength divided by the average AC breakdown strength of Mold. Moreover, the decrease in the laminating pitch from 0.1 to 0.05 mm improved the AC breakdown strength. Further, Print H_0.05mm had a 20% higher breakdown strength than that of Mold.

	Mold	Print H_ 0.1mm	Print V_ 0.1mm	Print H_ 0.05mm	Print H_ 0.05mm
Normalized AC breakdown strength	1.00	0.77	0.59	1.18	1.10

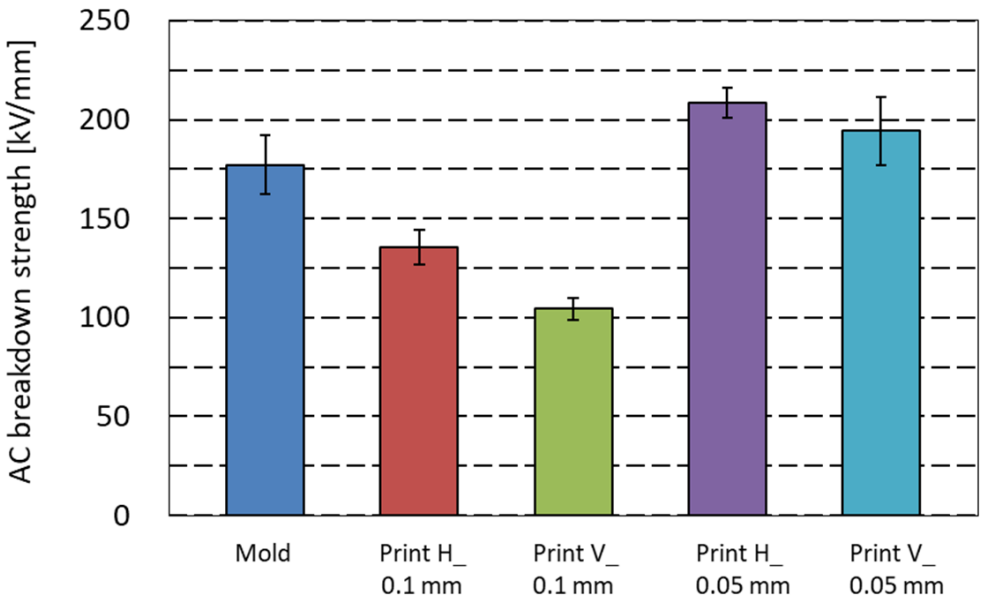

Fig.12 AC breakdown strengths of Mold, Print H_0.1mm, Print V_0.1mm, Print H_0.05mm, Print V_0.05mm.

Fig. 13 presents the normalized hardness of the 0.1 mm laminating pitch and 0.05 mm laminating pitch. The normalized hardness was obtained by dividing the hardness by the average hardness of the section of interest (the interface in each laminating pitch). The actual average-hardness are 2.27 MPa in 0.1 mm laminating pitch and 1.12 MPa in 0.05 mm laminating pitch. The difference in hardness depends on the slight difference in the measurement temperature, humidity and the surface state of the sample cross-section. Since the 0.1 mm laminating pitch and the 0.05 mm laminating pitch were tested on different days, they were normalized with the actual hardness, respectively. By lowering the laminating pitch to 0.05 mm, the difference in hardness between the part and the layer interface and between the layer interfaces was eliminated. The decrease in the laminating pitch thickness improved the curing degree. Therefore, it was concluded that sufficiently curing each layer and increasing the number of layers per sample thickness could enhance the breakdown strength of the 3D-printed insulator.

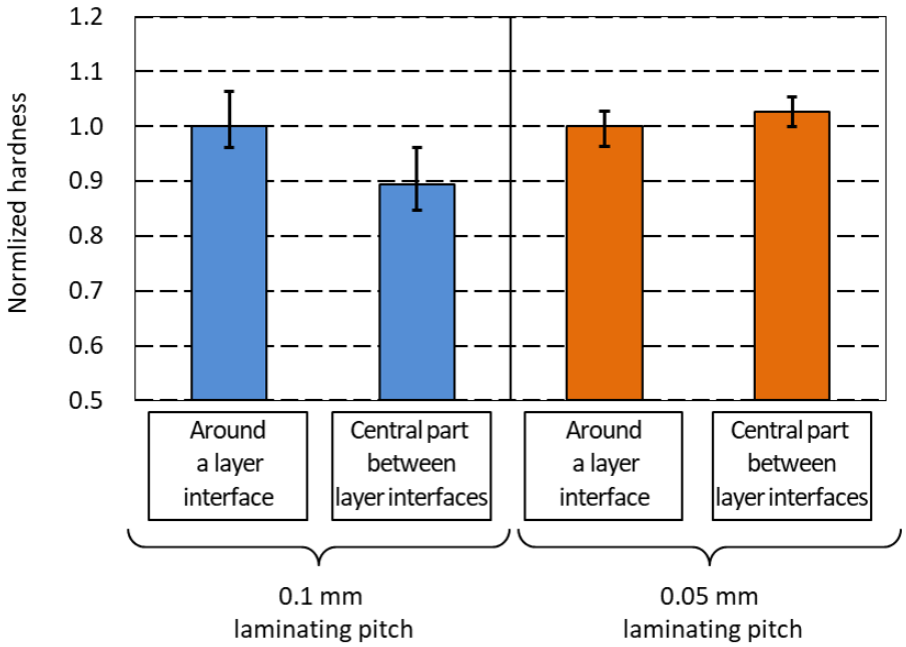

Fig.13 Normalized hardness of 0.1 mm laminating pitch and 0.05 mm laminating pitch.

3.5.2 Cylindrical printing for cable insulato

A 3D-printed cylindrical insulator (such as a cable insulator or cable joint) (Fig. 1) would contain a layer interface parallel to the electric field direction (Fig. 14(a)). The layer interfaces parallel to the electric field direction decreased the breakdown strength of the cylindrical insulator, while the layer interfaces perpendicular to the electric field direction did not affect the breakdown strength. In this section, a 3D-printed cylindrical insulator with layer interfaces perpendicular to the electric field direction is proposed (Fig. 14(b)).

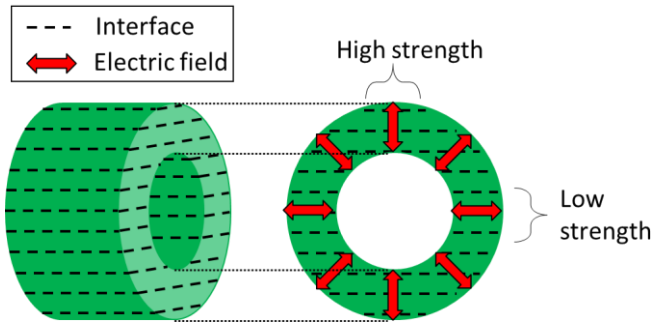

(a) Layer printing

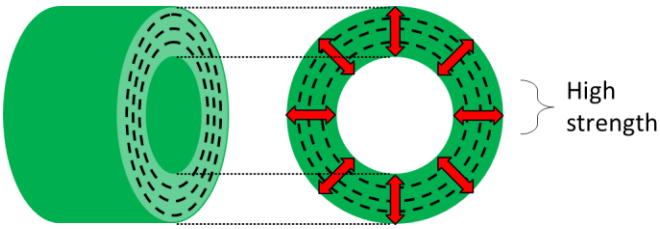

(b) Cylindrical printing

Fig.14 Layer printing and cylindrical printing for cable insulator.

Fig. 15 shows the structure of the 3D printer for the cylindrical insulator. The liquid acrylic rubber was irradiated with UV light while a motor drove the cylindrical metal rotor. After curing one layer, the metal rotor rose by 0.1 mm for the set pitch and laminated the second layer. The same operation was repeated to complete the cylindrical insulator. In the demonstration, a SUS pipe with an outside diameter of 22 mm was used as the rotor. The

materials used were acrylic rubber and resin. The tensile strength of the acrylic resin was 65 MPa. Further, the laminating pitch was set at 0.1 mm, and the rotational speed of the motor was maintained at 260 s/circumference. Fig. 16 shows the 3D-printed cylindrical insulators with layer interfaces perpendicular to the electric field direction. A cylindrical insulator of a 0.5 mm-thick (5-layer) acrylic rubber and a 1.5-mm-thick (15-layer) acrylic resin were used for 3D printing. Thus, a thick cylindrical insulator was simpler to make with acrylic resin because before curing, the resin had a lower viscosity.

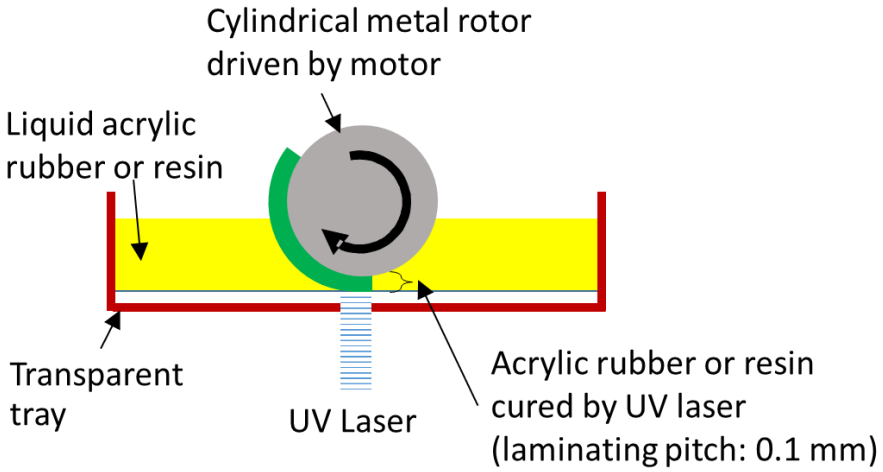

Fig. 15 Structure of the 3D printer for the cylindrical insulator.

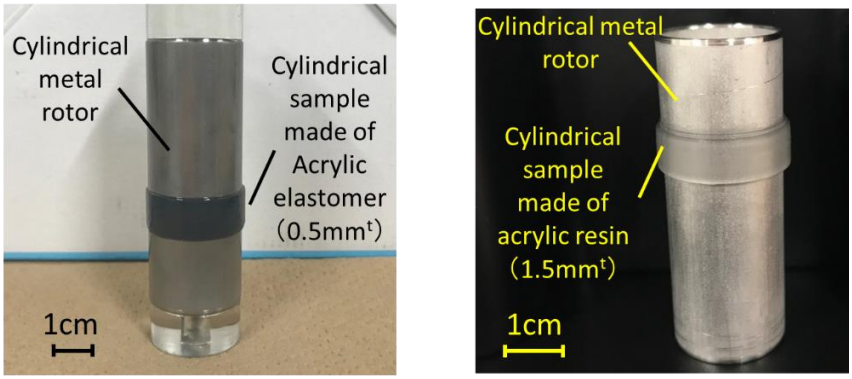

(a) Acrylic rubber material (b) Acrylic resin material

Fig. 16 3D-printed cylindrical insulators with the layer interfaces perpendicular to the electric field direction.

The breakdown strength of the cylindrical insulator of a 0.5 mm-thick (5-layer) acrylic rubber was tested. The purpose of this experiment is to verify that the breakdown strength of a cylindrical insulator is similar to that of a sheet sample (Print H_0.1 mm). We constructed an electrode system for breakdown test of a cylindrical insulator (Figure 17). A conductive tape connected to ground was attached to the surface of the cylindrical insulator. Epoxy molding and cone insulators were set to prevent the surface breakdown between the ground tape and the high voltage electrode.

AC breakdown strength of the cylindrical insulator was 27-42 kV/mm (N=6), which is different from the breakdown strength of the sheet sample (Print H_0.1 mm) evaluated by McKeown electrodes (86-170 kV/mm, N=10). This is because the electric-field-applied region of the cylindrical insulator is large and there are many breakdown points. The breakdown strength of the sheet samples (Print H_0.1 mm) evaluated by the parallel plate electrode with the same area of the electric-field-applied region as cylindrical insulator was 30-60 kV/mm (N=3). The cylindrical insulator has the breakdown strength similar to that of the sheet sample in the same area of the electric-field-applied region.

Figure 18 shows Weibull distribution of the breakdown strength of cylindrical insulator and sheet sample (Print H_0.1 mm). Each plot of the cylindrical insulator evinced a straight line, indicating that the breakdown phenomena of the cylindrical insulator agreed with Weibull probability. The inclination of the cylindrical insulator was similar in the order of Print H_0.1mm. It was observed that the effect of the layer interface on the breakdown strength of the cylindrical insulator prepared by cylindrical printing is similar to that of Print H_0.1 mm prepared by layer printing.

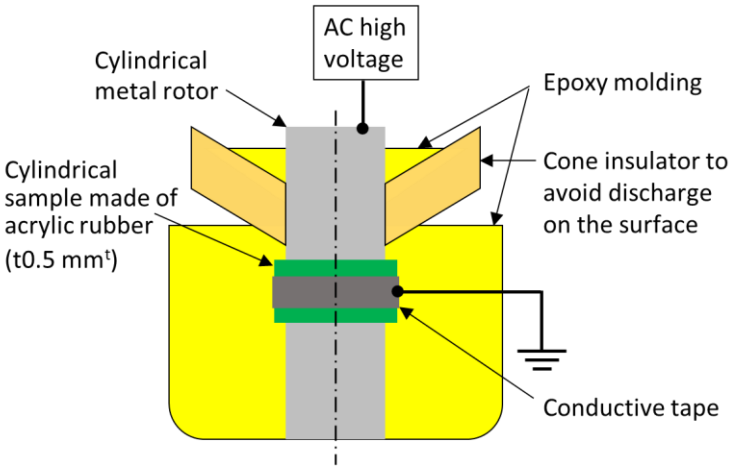

Fig. 17 An electrode system of a cylindrical insulator for breakdown test.

	Scale parameter	Shape parameter
Print H_0.1 mm(pitch)	147.4	5.0
Cylindrical insulator of a 0.5 mm-thick (5-layer) acrylic rubber (0.1mm pitch)	38.5	6.5

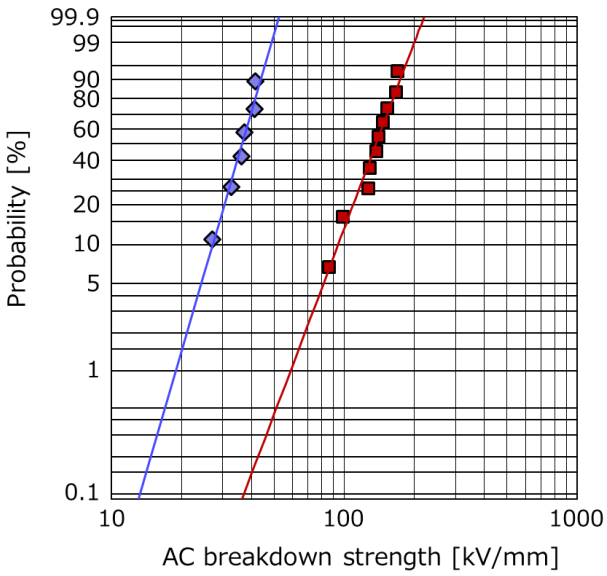

Fig. 18 Weibull distribution of AC breakdown strengths of the cylindrical insulator (a 0.5 mm-thick (5-layer) acrylic rubber) and Print H_0.1mm.

4. Conclusions

We investigated the layer interface effects on the dielectric breakdown strength of a 3D-printed acrylic rubber insulator with stereolithography. We compared the AC breakdown strength of insulators with different laminate directions. Furthermore, the morphology of the layer interfaces and the hardness in the vicinity of the interface were evaluated using microscopy and nanoindentation analyses. From our observations, we reached the following conclusions:

- The breakdown strength of the sheet sample of the 3D-printed acrylic rubber insulator with 0.1 mm laminating pitch was lower than that of the sheet sample without a laminate interface. We concluded that the layer interfaces with a laminating pitch of 0.1 mm reduced the AC breakdown strength of 3D-printed acrylic rubber insulators.
- There was no delamination or void around the layer interfaces, but the difference in hardness between the layer interface and the other part was observed.
- The difference in the material structure, due to insufficient curing near the layer interfaces, promoted dielectric breakdown.
- Further, 3D printing methods that minimize the layer interface effect on breakdown strength were demonstrated. The following results were obtained:
    - The decrease in the laminating pitch from 0.1 mm to 0.05 mm improved AC breakdown strength.
    - 3D-printed cylindrical insulators that minimize the negative layer interface effects on the breakdown strength was proposed and successfully formed.

Based on these conclusions, high-voltage engineers and researchers can focus on using a 3D printer to produce high-voltage insulators. Consequently, developing 3D-printed insulators for high-voltage applications and enabling an optimum shape and functionally graded structure

would be beneficial because of compactness and high reliability of power apparatus for use in power grids. In the future, we will develop a thicker sample and conduct dielectric breakdown tests for it.

References

[1] Makers: The New Industrial Revolution, Crown Business, 2012.

[2] B. Berman, 3-D printing: The new industrial revolution, Business Horizons 55 (2012) 155-162.

[3] W. Gao, Y. Zhang, D. Ramanujan, K. Ramani, Y. Chen, C. B. Williams, C. C. L. Wang, Y. C. Shin, S. Zhang, P. D. Zavattieri, The status, challenges, and future of additive manufacturing in engineering, Computer-Aided Design 69 (2015) 65-89.

[4] W. Gao, The status, challenges, and future of additive manufacturing in engineering, 69 (2015) 65-89.

[5] X. Wang, M. Jiang, Z. Zhou, J. Gou, D. Hui, 3D printing of polymer matrix composites: A review and prospective, Composites Part B: Engineering 110 (2017) 442-458.

[6] ASTM F2792-12a, "Standard Terminology for Additive Manufacturing"

[7] A.C. de Leon, Q. Chen, N. B. Palaganas, J. O. Palaganas, J. Manapat, R. C. Advincula, High performance polymer nanocomposites for additive manufacturing applications, Reactive and Functional, Polymers 103 (2016) 141-155.

[8] J. Manapat, Q. Chen, P. Ye, R. Advincula, 3D printing of polymernanocomposites via stereolithography, Macromol. Mater. Eng. (2016).

[9] J. Z. Manapat, Q. C. P. Ye, R. C. Advincula, 3D printing of polymer nanocomposites via stereolithography, Macromolecular Materials and Engineering 302 (9) (2017) 1600553.

[10] X. Wang, M. Jiang, Z. Zhou, J. Gou, D. Hui, 3D printing of polymer matrixcomposites: a review and prospective, Computer-Aided Des. Compos. Part B 110 (2017) 442-458.

[11] J. Z. Manapat, J. D. Mangadlao, B. D. B. Tiu, G. C. Tritchler, R. C. Advincula, High-strength stereolithographic 3D printed nanocomposites: graphene oxide metastability, ACS Appl. Mater. Interfaces 9 (2017) 10085-10093

[12] Z. Weng, Y. Zhou, W. Lin, T. Senthil, L. Wua, Structure-property relationship of nano enhanced stereolithography resin for desktop SLA 3D printer, Composites Part A: Applied Science and Manufacturing 88 (2016) 234-242.

[13] Y. Miyamoto, W. A. Kaysser, B. H. Rabin, A. Kawasaki, R. Ford, Functionally Graded Materials: Design, Processing, and Applications, Kluwer Academic, Osaka (1996).

[14] B. Kieback, A. Neubrand, H. Riedel, Processing techniques for functionally graded materials, Materials Science and Engineering: A 362 (2003) 81-106

[15] K. Kato, M. Kurimoto, H. Shumiya, H. Adachi, S. Sakuma, H. Okubo, Application of functionally graded material for solid insulator in gaseous insulation system, IEEE Trans. Dielectr. Electr. Insul. (13) 1 (2006) 362-372.

[16] M. Kurimoto, K. Kato, M. Hanai, Y. Hoshina, M. Takei, H. Okubo, Application of functionally graded material for reducing electric field on electrode and spacer interface, IEEE Trans. Dielectr. Electr. Insul. 17 (1) (2010) 256-263.

[17] A. Garland, G. Fadel, Design and manufacturing functionally gradient material objects with an off the shelf three-dimensional printer: challenges and solutions, Journal of Mechanical Design 137 (2015) 111407-1-11, 2015

[18] D. V. Kaweesa, N. A. Meisel, Quantifying fatigue property changes in material jetted parts due to functionally graded material interface design, Additive Manufacturing 21 (2018) 141-149.

[19] M. Kurimoto, H. Ozaki, T. Sawada, T. Kato, T. Funabashi, Y. Suzuoki, Filling ratio control of TiO2 and SiO2 in epoxy composites for permittivity-graded insulator with low coefficient of thermal expansion, IEEE Trans. Dielectr. Electr. Insul. 25 (3) (2018) 1112-1120.

[20] M. Kurimoto, H. Ozaki, Y. Yamashita, T. Funabashi, T. Kato, Y. Suzuoki, Dielectric properties and 3D printing of UV-cured acrylic composite with alumina microfiller, IEEE Trans. Dielectr. Electr. Insul. 23 (5) (2016) 2985-2992.

[21] X.-R. Li, Z. Liu, W.-D. Li, G.-Y. Sun, J.-Y. Xue, C. Wang, G.-J. Zhang, 3D printing fabrication of conductivity non-uniform insulator for surface flashover mitigation, IEEE Trans. Dielectr. Electr. Insul. 26 (4) (2019) 1172-1180.

[22] W.J. Monzel, B. W. Hoff, S. S. Maestas, D. M. French, S. C. Hayden, Dielectric breakdown of additively manufactured polymeric materials, IEEE Transactions on Dielectrics and Electrical Insulation 22 (6) (2015) 3543-3549.

[23] B. W. Hoffa, S. S. Maestas, S. C. Hayden, D. J. Harrigan, R. O. Grudt, M. L. Ostraat, J. C. Horwath, S. Leontsev, Dielectric strength heterogeneity associated with printing orientation in additively manufactured polymer materials, Additive Manufacturing 22 (2018) 21-30, 2018.

[24] S. Iwata, R. Kitani, Influence of surface roughness of additive manufacturing polymer on surface flashover voltage, Electrical Engineering 100 (2018) 1949-1955.

[25] H. Kodama, Automatic method for fabricating a three-dimensional plastic model with photo-hardening polymer, Rev. Scientific Instrum. 52 (11) (1981) 1770-1773.

[26] J. Dulieu-Barton, M. Fulton, Mechanical properties of a typical stereolithography resin, Strain Int. J. Exp. Mech. 36 (2) (2000) 81-87.

[27] K. Chockalingam, N. Jawahar, U. Chandrasekar, K. Ramanathan, Establishment of process model for part strength in stereolithography, J. Mater. Process. Technol. 208 (2008) 348-365.

[28] J. J. McKeown, Intrinsic electric strength of organic polymeric materials, Proc. IEEE 112 (4) (1965) 824-828.

[29] ASTM D149-09, Standard Test Method for Dielectric Breakdown Voltage and Dielectric Strength of Solid Electrical Insulating Materials at Commercial Power Frequencies, West Conshohocken, PA (2013) www.astm.org.

[30] C. Laurent, C. Chauvet, J. Berdala, The significance of the weibull threshold in short-term breakdown statistics, IEEE Trans. Dielectr. Electr. Insul. 1 (1) (1994) 160-162.

[31] D. Fabiani, L. Simoni, Discussion on application of the weibull distribution to electrical breakdown of insulating materials, IEEE Trans. Dielectr. Electr. Insul. 12 (1) (2005) 11-16.

[32] S. Pelissou, H. St-Onge, M. R. Wertheimer, Dielectric breakdown in polyethylene at elevated temperatures, IEEE Trans. Dielectr. Electr. Insul. 19 (3) (1984) 241-244.

[33] Seitz, F.: Phys. Rev., Vol.76, (1949) 1376-1393